Journal of Materials Chemistry C

PAPER

View Article Online
View Journal | View Issue

Cite this: J. Mater. Chem. C, 2018, 6, 1573

Morphology control towards bright and stable inorganic halide perovskite light-emitting diodes†

Fangming Jin,[a] Bo Zhao,*[bc] Bei Chu,[a] Haifeng Zhao,[a] Zisheng Su,*[ad] Wenlian Li[a] and Furong Zhu*[c]

Received 11th October 2017,
Accepted 10th January 2018

DOI: 10.1039/c7tc04631f

rsc.li/materials-c

The effect of morphology control on the performance of inorganic cesium lead halide based green perovskite light-emitting diodes (PeLEDs) was analyzed. PeLEDs were prepared using two different formulation approaches: (1) the solution was prepared by dissolving $CsPbBr_3$ powders in dimethyl sulfoxide (DMSO), and (2) the precursor solution was formulated by dissolving CsBr and $PbBr_2$ powders with different molar ratios of CsBr to $PbBr_2$ in DMSO. A peak luminance of 4590 cd m^{-2} was obtained for the PeLEDs prepared with $CsPbBr_3$-solution, which is 48 and 12 times higher than that of the optimized PeLEDs fabricated using CsBr/$PbBr_2$ precursor solutions with different molar ratios of CsBr to $PbBr_2$ of 2 : 1 and 1 : 1. Our results reveal that the morphology and control of excess Pb atoms in the perovskite emitting layer play an important role in modulating the current losses and the radiative decay rate, which were optimized in this work for attaining efficient operation of the PeLEDs.

1. Introduction

Recently, organic–inorganic hybrid perovskites have attracted increasing attention for application in photovoltaic devices due to their low cost, earth-abundance and solution-fabrication processes at low temperatures under ambient conditions. Rapid progress has been made in perovskite solar cells with a power conversion efficiency of above 20%.[1–4] Organic–inorganic hybrid perovskites are also emerging as a promising technology for use in light-emitting diodes (LEDs) because they can provide high color purity with a full width at half maximum (FWHM) of ~20 nm irrespective of their crystal size. Unlike the conventional inorganic quantum dots, their intrinsic crystal structure is like a multiple quantum well.[5–10] The perovskite nanoparticles have a high photoluminescence quantum yield (PLQY). Reports on the progress of organic–inorganic hybrid perovskite LEDs increased rapidly in less than one year, *e.g.*, bilayered perovskite light-emitting diodes (PeLEDs) with a high current efficiency of 42.9 cd A^{-1} were demonstrated.[11] More recently, LEDs based on all solution-processable inorganic perovskites have also attracted considerable research interest because of the advantages of high PLQY, easily tunable emission colors, and high color purity for applications in solid-state lighting and displays.[12–15] Solution-processed inorganic $CsPbBr_3$-based perovskite LEDs, fabricated using CsBr–$PbBr_2$ precursor solutions with two different CsBr/$PbBr_2$ molar ratios of 2 : 1 and 1 : 1, with maximum luminance values of 407 cd m^{-2} and 132 cd m^{-2} were demonstrated.[12] The performance of $CsPbBr_3$-based PeLEDs remains modest, due to the incomplete surface coverage of perovskite films and exciton quenching caused by the excess interstitial Pb atoms. The presence of the excess Pb atoms deteriorates the luminance because of the increase in the nonradiative decay rate, thereby causing a decrease in the radiative decay rate.[16] The existence of interstitial Pb atoms in a pure inorganic perovskite is more severe than that in organic–inorganic hybrid perovskites due to the lower solubility of CsBr than that of the methylammonium halide (MABr) in solution. Interstitial Pb atoms can emerge in $MAPbBr_3$ even if MABr and $PbBr_2$ are mixed at a molar ratio of 1 : 1 because of the unintended losses of Br atoms or the incomplete reaction between MABr and $PbBr_2$.[17] In a pure inorganic perovskite, the stoichiometric ratio of CsBr to $PbBr_2$ is less than 1 : 1 because of the low solubility of CsBr in solvents such as dimethylformamide (DMF) or dimethyl sulfoxide (DMSO), leading to a much higher excess of interstitial Pb atoms in the perovskite layer. Simultaneous reduction of the concentrations of $PbBr_2$ and CsBr seems to be an effective method to decrease the ratio of $PbBr_2$ to CsBr in the perovskite. However, reducing the concentrations of precursors in the

[a] State Key Laboratory of Luminescence and Applications, Changchun Institute of Optics, Fine Mechanics and Physics, Chinese Academy of Sciences, Changchun 130033, China. E-mail: suzs@ciomp.ac.cn
[b] Key Laboratory of Interface Science and Engineering in Advanced Materials of Ministry of Education, Research Center of Advanced Materials Science and Technology, Taiyuan University of Technology, Taiyuan 030024, China. E-mail: zhaobo01@tyut.edu.cn
[c] Department of Physics, Institute of Advance Materials, and Institute of Research and Continuing Education (Shenzhen), Hong Kong Baptist University, Hong Kong, China. E-mail: frzhu@hkbu.edu.hk
[d] College of Physics and Information Engineering, Quanzhou Normal University, Quanzhou 362000, China

† Electronic supplementary information (ESI) available. See DOI: 10.1039/c7tc04631f

formulations results inevitably in a decrease in the perovskite layer thickness, a poorer surface coverage of the perovskite film, and thereby a much higher current loss. These are two limiting factors and remain an open challenge for further improvement in the performance of inorganic perovskite-based PeLEDs.

In this work, the effect of morphology and the presence of interstitial Pb atoms on the performance of inorganic cesium lead halide perovskite based green PeLEDs was analyzed. Our results reveal that the morphology of the perovskite film and the amount of interstitial lead atoms closely relate to the efficient operation of PeLEDs, and they can be controlled by adjusting the perovskite precursor solution. Morphology control provides an optimal coverage and effective blocking of pinholes or electrical shunting paths with a smaller perovskite crystal. The formation of interstitial Pb atoms, which is closely associated with strong exciton quenching, can be suppressed by optimizing the perovskite precursor solution. PeLEDs with low current losses and a higher radiative decay rate were attained by the morphology control and suppression of interstitial Pb atoms in the perovskite light-emitting layer, approaching a peak brightness of 4590 cd m^{-2}, which is 11 times higher than that reported for similar PeLEDs,[12] and also is 48 and 12 times higher than reference devices made with $CsBr/PbBr_2$ precursor solutions having different molar ratios of 2 : 1 and 1 : 1.

2. Experimental section

2.1 Synthesis of $CsPbBr_3$ powders

$CsPbBr_3$ powders were synthesized following the procedure reported in the literature.[18] Firstly, $PbBr_2$ powders (7.31 g, 20 mmol) were dissolved in 30 ml of 48% aqueous HBr to form a pale-yellow solution. Secondly, CsBr (4.26 g, 20 mmol) powders were dissolved in 10 ml of H_2O. The precipitation of a bright orange solid appeared by mixing the $PbBr_2$ and CsBr solutions. Finally, the solid was suction filtered, washed copiously with absolute EtOH and dried under vacuum to obtain >10 g of pure $CsPbBr_3$ powders, with a yield of >90%. The X-ray diffraction (XRD) patterns and the photograph taken of the $CsPbBr_3$ powders thus synthesized are shown in Fig. S1 (ESI†).

2.2 Device fabrication

All the materials used for device fabrication were purchased from commercial sources and used without further purification except for the $CsPbBr_3$ powders, which were synthesized in-house in this work. Indium tin oxide (ITO)-coated glass substrates with a sheet resistance (R_s) of 15 Ω sq^{-1} were cleaned by ultra-sonication in acetone, detergent, and acetone, and the ITO/glass substrates were then exposed to ultraviolet zone for 10 min prior to device fabrication. PEDOT:PSS was spin-coated onto ITO/glass at a rotation speed of 3500 rpm for 50 s and annealed in air at 120 °C for 20 min. 200 nm thick $CsPbBr_3$ perovskite films were formed on PEDOT:PSS using different $CsPbBr_3$ solutions, *e.g.*, solution A (dissolving 0.55 M $CsPbBr_3$ in DMSO), solution B (filtered solution with a molar ratio of CsBr to $PbBr_2$ of 1 : 1 in DMSO) and solution C (filtered solution with a molar ratio of CsBr to $PbBr_2$ of 2 : 1 in DMSO), by spin-coating at a rotation speed of 1500 rpm for 70 s. 5 wt% 4,7-diphenyl-1,10-phenanthroline (BPhen) in chloroform was dropped immediately on the surface of the $CsPbBr_3$ perovskite film for 30 s to reduce the crystal size. The samples were then baked at 90 °C for 10 min and transferred into a high-vacuum chamber (with a base pressure of $\sim 3 \times 10^{-4}$ Pa) for the preparation of a 50 nm thick BPhen and 80 nm thick Ag (80 nm) bilayer contact sequentially by thermal deposition at deposition rates of 1 and 3 Å s^{-1}, respectively.

2.3 Characterization

The current density–voltage–luminance characteristics of the PeLEDs were measured using a Keithley model 2400 power supply combined with a ST-900M spot photometer, and were recorded simultaneously during the measurements. The absorption spectra of the perovskite layers were measured using a Shimadzu UV-3101PC spectrophotometer. Steady-state photoluminescence (PL) spectra of the perovskite films were measured using a Hitachi F7000 fluorescence spectrophotometer. The electroluminescence (EL) spectra of the PeLEDs were measured using an OPT-2000 spectrophotometer. Scanning electron microscopy (SEM) images of the perovskite layers were obtained using a Hitachi S4800 field emission scanning electron microscope. XRD patterns of the perovskite films were recorded with a Rigaku D/Max-2500 diffractometer using Cu Kα radiation (λ = 1.54 Å). The PeLEDs were not encapsulated and were measured in air at room temperature.

3. Results and discussion

PeLEDs have a multilayer structure of ITO/PEDOT:PSS (~40 nm)/$CsPbBr_3$ (~200 nm)/BPhen (50 nm)/silver (Ag 80 nm), and the schematic cross-sectional view of the PeLEDs is shown in Fig. 1a. The corresponding schematic flat-band energy level diagram of the devices is shown in Fig. 1b. The 50 nm thick wide bandgap BPhen layer was employed to serve as an electron transporting layer and a hole blocking layer, because of its excellent optical transparency and shallow conduction-band energy level. PEDOT:PSS was used as a hole transporting layer and an electron blocking layer. Three types of PeLEDs, defined as Device-A, Device-B and Device-C, were prepared using different $CsPbBr_3$ formulation solutions, *e.g.*, "Device-A" type PeLEDs were fabricated using perovskite solution formulated by dissolving 0.55 M synthesized $CsPbBr_3$ powders in DMSO (precursor-A). The

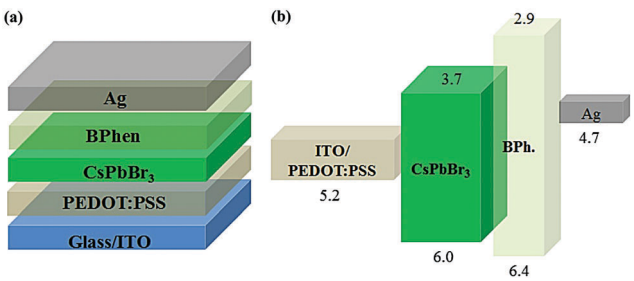

Fig. 1 (a) Schematic cross-sectional view and (b) schematic energy-level diagram of the PeLEDs.

$CsPbBr_3$ powders can be dissolved sufficiently in DMSO forming a clear and transparent solution after annealing at 70 °C for 20 min. "Device-B" and "Device-C" types of PeLEDs were fabricated using precursor solutions formulated by blending CsBr and $PbBr_2$ in DMSO with different molar ratios of 1 : 1 (precursor-B) and 2 : 1 (precursor-C). Due to the inferior solubility of CsBr, precipitates were formed in both precursor-B and precursor-C solutions. The photographs taken for different perovskite formulation solutions of precursor-A, precursor-B and precursor-C are shown in Fig. S2 (ESI†), showing that precursor B has a pale-yellow color and precursor-C has a yellowish color due to the presence of excess interstitial Pb atoms in the $CsPbBr_3$ solution, suggesting the stoichiometric ratio of CsBr to $PbBr_2$ in the precursor solution is less than 1 : 1. The cross-sectional SEM images taken for the perovskite layers on PEDOT:PSS fabricated from different perovskite formulation solutions of precursor-A, precursor-B and precursor-C are presented in Fig. S3 (ESI†). These $CsPbBr_3$ samples have a similar layer thickness of about 200 nm, revealing that the concentration of $PbBr_2$ in the solutions dominates the perovskite film thickness. The huge surface roughness comes from the large crystal size, forming voids between the crystals and thereby a low surface coverage. The crystal structures of the $CsPbBr_3$ perovskite films prepared by three different formulations were analyzed using XRD measurements. The XRD patterns measured for the perovskite films prepared from three different solutions are given in Fig. S4 (ESI†), revealing that all films consist of polycrystalline $CsPbBr_3$ phases.[18] It can be seen from the XRD patterns that the change in the stoichiometric ratio of CsBr to $PbBr_2$ in the solutions had very little effect on the crystallinity of the resulting $CsPbBr_3$ perovskite films.

UV-vis absorption and PL spectra measured for the $CsPbBr_3$ perovskite film prepared from precursor-A are shown in Fig. 2a. The absorption peak of the perovskite film is located at 515 nm, while the position of the PL emission peak is at around 532 nm, with a narrow FWHM of 18 nm, in agreement with results reported previously for $CsPbBr_3$-based green PeLEDs.[12] The UV-vis absorption and PL spectra of perovskite films formed using precursor-B and precursor-C solutions are similar to that measured for the film papered from precursor-A solution, as shown in Fig. S5 (ESI†). The non-zero baseline in the absorption spectra can be attributed to light scattering and interference effects. The EL spectra measured for all the perovskite devices are plotted in Fig. 2b. The PeLEDs prepared from three different formulation solutions exhibit almost the same emission behavior, which implies that the light-emission occurred from a $CsPbBr_3$-based perovskite emitter and no emission from the interface material occurred. The EL peaks located at 527 nm have a FWHM of 21 nm, which is similar to the PL spectra of these $CsPbBr_3$ films.

The SEM images measured for the $CsPbBr_3$ perovskite films prepared from different solutions of precursor-A, precursor-B and precursor-C are shown in Fig. 3. Perovskite layers with micrometer-sized $CsPbBr_3$ domains were scattered on the PEDOT:PSS surface prepared with the precursor-B and precursor-C solutions. A large amount of volume remained unfilled because the perovskite layers were not fully occupied by the $CsPbBr_3$ cuboids. This high

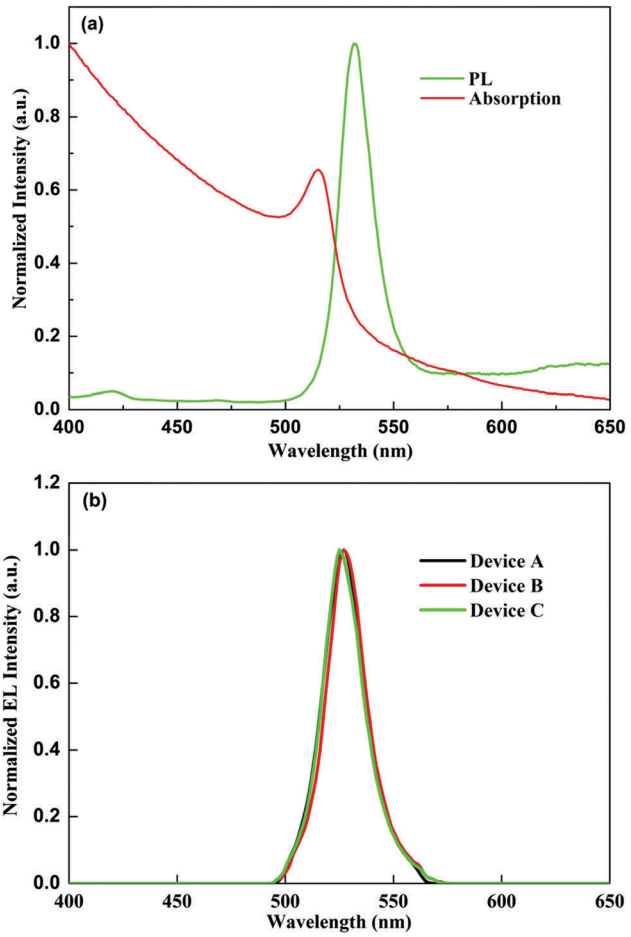

Fig. 2 (a) Absorption and PL spectra measured for the perovskite film prepared using precursor-A solution (365 nm excitation wavelength). (b) Normalized EL spectra measured for PeLEDs prepared from different perovskite formulation solutions of precursor-A, precursor-B and precursor-C.

surface roughness and the formation of pinholes in inorganic halide perovskite films result in the formation of a poor interface with the electron transport layer forming electrical shunt paths, which severely limit the current efficiency in PeLEDs. In contrast, for the $CsPbBr_3$ perovskite film prepared with precursor-A solution, a perfect surface coverage was obtained and the $CsPbBr_3$ crystal morphology changed to a well-packed assembly of tiny grains ranging from 100 to 250 nm, as shown in Fig. 3a and d. The smaller grains can spatially limit the diffusion length of excitons and reduce the possibility of exciton dissociation into carriers. 95% coverage of the $CsPbBr_3$ perovskite was obtained for the film prepared with precursor-A solution, estimated based on SEM images using Image J software, which is much higher than that of the films prepared with the precursor-B solution ($\approx$80%) and precursor-C solutions ($\approx$70%). The pinholes in the perovskite films caused by incomplete surface coverage lead to substantial nonradiative current losses. We propose that the difference in the morphology of the perovskite films fabricated with different precursor solutions originates from different stoichiometric ratios of CsBr to $PbBr_2$ in the films, where an excess of $PbBr_2$ seems to favor large crystal formation in the film growth progress.[19]

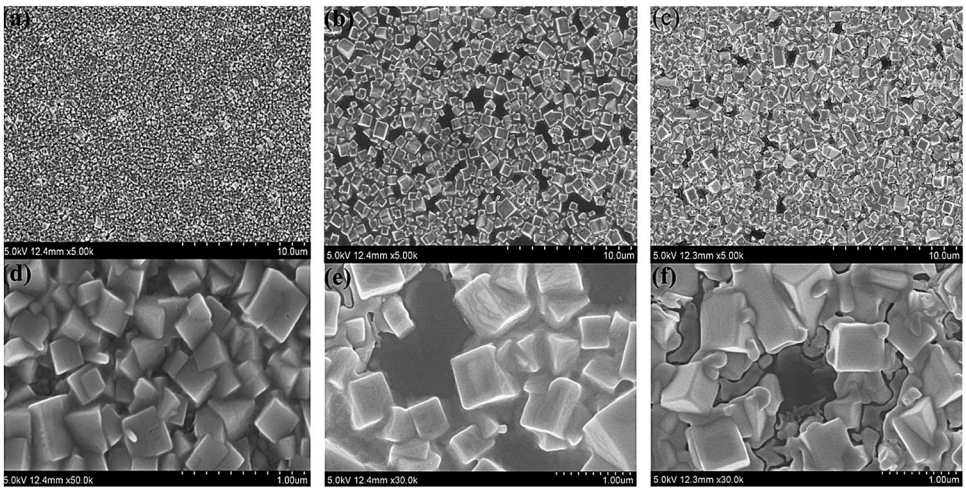

Fig. 3 The SEM images taken for $CsPbBr_3$ perovskite films prepared from different formulation solutions of precursor-A, (a) and (d), precursor-B (b and e), and precursor-C (c and f).

The current density–voltage–luminance characteristics of the PeLEDs are presented in Fig. 4a. The EL performance of the PeLEDs is summarized in Table 1. It shows that the optimal morphology improves the crystallization quality and helps to improve the conductivity, contributing to a significant improvement in the current density of Device-A, agreeing with the phenomenon reported previously.[12] The reference devices of "Device-B" and "Device-C" PeLEDs had a maximum luminance of 92 cd m^{-2} and 337 cd m^{-2}, respectively, similar to a maximum luminance of 132 cd m^{-2} reported for the device made with a molar ratio of CsBr to $PbBr_2$ of 1 : 1 in the precursor solution and a maximum luminance of 407 cd m^{-2} for PeLEDs fabricated with a molar ratio of CsBr to $PbBr_2$ of 2 : 1. "Device-A" type PeLEDs had the lowest turn-on voltage of 2.8 V as compared to 4.2 V for Device-B and 3.7 V for Device-C. Notably, pure green emission can be observed from Device-A at an operating voltage as low as 2.8 V, indicating that an efficient charge injection into the $CsPbBr_3$ perovskite emitting layer was achieved. In the present experiments, an increased current efficiency and an external quantum efficiency (EQE) were observed with both increased voltage and current density, which are shown in Fig. 4b. The current efficiency and EQE of the green PeLEDs increase with an increase in current density due to a dominant radiative bimolecular recombination at higher excitation densities. The EQE of the best-performing "Device-A" type PeLEDs reaches up to $\approx$0.06% at the highest luminance of 4590 cd m^{-2} with a current density of 1830 mA cm^{-2}, where a highest current efficiency of 0.25 cd A^{-1} is also achieved. The maximum luminance, current efficiency and EQE of Device-A are 48, 28 and 29 times higher than those measured for Device-B, and 12, 21 and 19 times higher than those of Device-C. It was reported that a reduced trap density could account for the improved performance of PeLEDs fabricated using a CsBr-rich solution.[12] We show here that this is not the whole reason. Compared to the CsBr-rich film, there exist many more pinholes in the perovskite film fabricated by the equimolar CsBr–$PbBr_2$ solution as shown in the SEM images. The poor coverage of the film

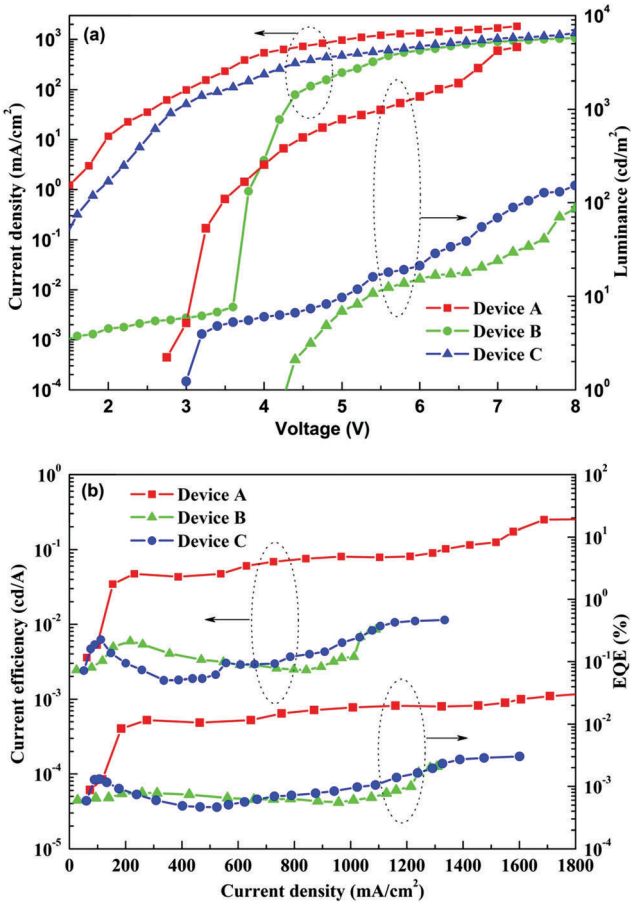

Fig. 4 (a) Current density–voltage–luminance characteristics, (b) current efficiency–current density–EQE characteristics measured for three types of PeLEDs prepared using different formulation solutions of precursor-A, precursor-B and precursor-C.

fabricated by the equimolar CsBr–$PbBr_2$ solution must result in a large amount of electrical shunting paths and induce serious current losses, which lead to inferior device performances in

Table 1 A summary of the performance of different PeLEDs

Samples	$V_{turn\text{-}on}$ (V)	L_{max} (cd m^{-2})	Current efficiency (cd A^{-1})	EQE$_{max}$ (%)
Device-A	2.8	4590	0.25	0.06
Device-B	4.2	92	0.0085	0.002
Device-C	3.7	337	0.011	0.003

luminance, current efficiency and EQE. We also found that that breakdown is much easier for Device-B and Device-C than Device-A at the same current density, which is attributed to the local Joule heating from the high current filament through the pinholes. This is in accordance with the device working lifetime test. As shown in Fig. 5, the emission from a non-encapsulated Device-A can remain for more than half an hour, while breakdown in a few seconds was observed for Device-B and Device-C types of PeLEDs. Hence, the pinholes in the perovskite films limit the device EQE through nonradiative current losses, as well as limit the maximum brightness of the PeLEDs by causing early breakdown at low bias voltages. In addition, the number of excess interstitial Pb atoms is much lower in Device-A as compared to that in Device-B due to the poor solubility of CsBr in the precursor solution, as shown in Fig. S2 (ESI†). The relatively low density of the excess interstitial Pb atoms in Device-A reduces the exciton quenching probability, which is beneficial for promoting radiative recombination processes, and thereby enhances luminescence efficiency eventually.

The EL spectra of "Device-A" type PeLEDs at different drive voltages are shown in Fig. 6a, indicating that the EL spectra of the PeLEDs are not dependent on the external bias. The device gives a very narrow EL spectrum, arising from the band-edge emission. The PeLEDs display EL spectra solely from $CsPbBr_3$ without any noticeable contribution from any charge transport materials, indicating that the $CsPbBr_3$ emitter serves as the primary exciton recombination zone during device operation. The corresponding Commission Internationale de l'Eclairage (CIE) color coordinates of (0.16, 0.78) for the PeLEDs are shown in Fig. 6b, satisfying the requirement of the CIE coordinates for application in displays. The inset of Fig. 6b shows the photograph taken for a Device-A emitting pleasant green light, showing the uniform emission across the entire device pixel, demonstrating the emission quality and the potential of the $CsPbBr_3$-based PeLEDs made with a solution-fabrication process.

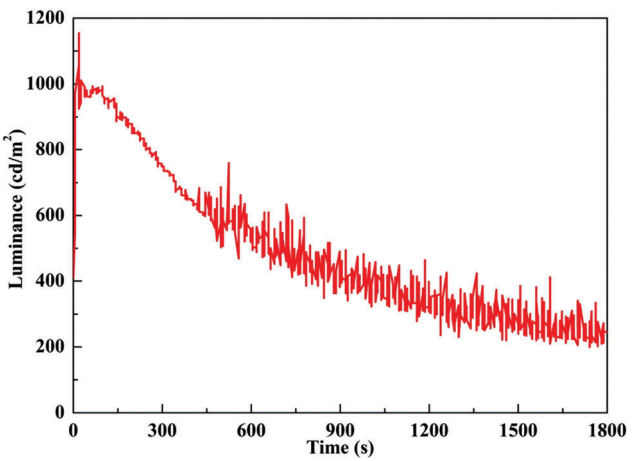

Fig. 5 Luminance–aging time characteristics measured for Device-A type PeLEDs under a constant operation voltage of 6 V.

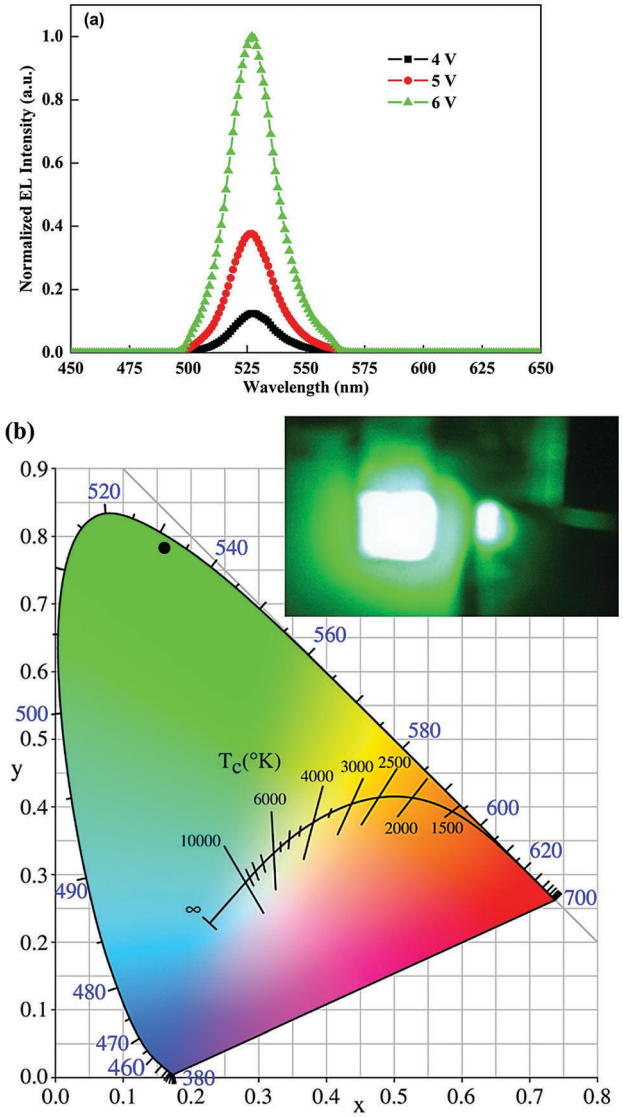

Fig. 6 (a) The EL spectra measured for Device-A type PeLEDs at different driving voltages of 4 V, 5 V and 6 V. (b) The CIE coordinates for the EL spectrum of Device-A operated at 6 V. Inset: Photographtaken for a working Device-A emitting green light.

It is necessary to note that device performance can be further optimized by interface engineering such as replacing the charge transfer layer of PEDOT:PSS. A high hole injection barrier exists at the PEDOT:PSS/perovskite interface because of the mismatch between the ionization potential (IP) level of the perovskite (~6.0 eV) and the work function (WF) of PEDOT:PSS (*ca.* 5.2 eV). This large hole injection barrier (~0.8 eV) limits hole injection into the perovskite layer and hence the overall electron–hole current balance in the emitting layer (EML). The PEDOT:PSS hole transporting layer also induces significant exciton quenching at the PEDOT:PSS/$CsPbBr_3$ interface because

of the long exciton diffusion length in the perovskite layer, and thereby reduces the device efficiency by limiting the radiative recombination of charge carriers.[20,21] Therefore, using a high-WF hole injection material enables prevention of exciton quenching in PeLEDs, which is of prime importance to achieve high EL performance by a combination of removing a high hole injection barrier and suppressing luminescence quenching. It was found that there existed an unintended loss of Br atoms in the perovskite layers, *e.g.*, the molar ratio of CsBr to $PbBr_2$ is less than 1 : 1 even in the perovskite films prepared from precursor-A solutions. The excess Pb atoms would induce strong exciton quenching. In the organic–inorganic hybrid perovskite LEDs, the maximum current efficiency can be varied from 4.87×10^{-2} to 21.4 cd A^{-1} by increasing the molar ratio of CH_3NHBr_3 to $PbBr_2$ from 1 : 1.05 to 1.05 : 1.[11] It is anticipated that the performance of the PeLEDs developed in this work can be further improved by introducing a small amount of CsBr in the precursor-A solution. Analyses of device performance and morphological characterization suggest that the $CsPbBr_3$ film prepared by precursor-A solution provides smaller crystalline grains and an optimal surface coverage, which effectively prevents the formation of pinholes or electrical shunting paths, and suppression of the excess interstitial Pb atoms. The combined effects avoid low current and losses to nonradiative decay leading to a significant enhancement in device efficiency.

4. Conclusion

In summary, the performance of inorganic cesium lead halide perovskite based green PeLEDs was analyzed. We found that the smooth morphology and the reduction of the excess interstitial Pb atoms in the perovskite emitter play an important role in the efficient operation of PeLEDs. The quality of the perovskite emitter was controlled by optimizing the formulation of the perovskite precursor solution. Morphology and excess interstitial Pb atoms are closely associated with the surface coverage of the perovskite emitter, which was optimized for preventing the formation of pinholes, electrical shunting paths and low current losses. The remarkable improvement in the EL performance of solution-processed PeLEDs was demonstrated. The outcomes of this work offer an attractive option toward low cost and solution-processable inorganic PeLEDs for applications in large-area displays and solid-state lighting.

Conflicts of interest

There are no conflicts to declare.

Acknowledgements

This work was supported by the National Natural Science Foundation of China (Grants 61604149, 61376062, 61376022, 61575192 and 61504145); the Science and Technology Development Plan of Jilin Province (20170520130JH and 20140101094JC); the Project of Jiangsu Key Laboratory for Carbon-Based Functional Materials and Devices (KJS1615); the Hong Kong Baptist University Faculty Research Grant (FRG2/2016-17/088); the Interinstitutional Collaborative Research Scheme (RC-ICRS/15-16/04); and the Shenzhen Peacock Plan (KQTD20140630110339343).

Notes and references

1 J. Burschka, N. Pellet, S. J. Moon, R. H. Baker, P. Gao, M. K. Nazeeruddin and M. Gratzel, *Nature*, 2013, **499**, 316.
2 H. S. Kim, C. R. Lee, J. H. Im, K. B. Lee, T. Moehl, A. Marchioro, S. J. Moon, R. H. Baker, J. H. Yum, J. E. Moser, M. Gratzel and N. G. Park, *Sci. Rep.*, 2012, **2**, 591.
3 M. M. Lee, J. Teuscher, T. Miyasaka, T. N. Murakami and H. J. Snaith, *Science*, 2012, **338**, 643.
4 H. Zhou, Q. Chen, G. Li, S. Luo, T. B. Song, H. S. Duan, Z. Hong, J. You, Y. Liu and Y. Yang, *Science*, 2014, **345**, 542.
5 V. D'Innocenzo, A. R. Srimath Kandada, M. D. Bastiani, M. Gandini and A. Petrozza, *J. Am. Chem. Soc.*, 2014, **136**, 17730.
6 R. L. Hoye, M. R. Chua, K. P. Musselman, G. Li, M. L. Lai, Z. K. Tan, N. C. Greenham, J. L. MacManus-Driscoll, R. H. Friend and D. Credgington, *Adv. Mater.*, 2015, **27**, 1414.
7 Y. H. Kim, H. Cho, J. H. Heo, T. S. Kim, N. Myoung, C. L. Lee, S. H. Im and T. W. Lee, *Adv. Mater.*, 2015, **27**, 1248.
8 G. Li, Z. K. Tan, D. Di, M. L. Lai, L. Jiang, J. H. Lim, R. H. Friend and N. C. Greenham, *Nano Lett.*, 2015, **15**, 2640.
9 J. Li, S. G. Bade, X. Shan and Z. Yu, *Adv. Mater.*, 2015, **27**, 5196.
10 J. Wang, N. Wang, Y. Jin, J. Si, Z. K. Tan, H. Du, L. Cheng, X. Dai, S. Bai, H. He, Z. Ye, M. L. Lai, R. H. Friend and W. Huang, *Adv. Mater.*, 2015, **27**, 2311.
11 H. Cho, S. H. Jeong, M. H. Park, Y. H. Kim, C. Wolf, C. L. Lee, J. H. Heo, A. Sadhanala, N. Myoung, S. Yoo, S. H. Im, R. H. Friend and T. W. Lee, *Science*, 2015, **350**, 1222.
12 N. Yantara, S. Bhaumik, F. Yan, D. Sabba, H. A. Dewi, N. Mathews, P. P. Boix, H. V. Demir and S. Mhaisalkar, *J. Phys. Chem. Lett.*, 2015, **6**, 4360.
13 X. Zhang, H. Lin, H. Huang, C. Reckmeier, Y. Zhang, W. C. Choy and A. L. Rogach, *Nano Lett.*, 2016, **16**, 1415.
14 J. Song, J. Li, X. Li, L. Xu, Y. Dong and H. Zeng, *Adv. Mater.*, 2015, **27**, 7162.
15 L. Protesescu, S. Yakunin, M. I. Bodnarchuk, F. Krieg, R. Caputo, C. H. Hendon, R. X. Yang, A. Walsh and M. V. Kovalenko, *Nano Lett.*, 2015, **15**, 3692.
16 E. Dulkeith, M. Ringler, T. A. Klar, J. Feldmann, A. M. Javier and W. J. Parak, *Nano Lett.*, 2005, **5**, 585.
17 R. Sheng, A. H. Baillie, S. Huang, S. Chen, X. Wen, X. Hao and M. A. Green, *J. Phys. Chem. C*, 2015, **119**, 3545.
18 C. C. Stoumpos, C. D. Malliakas, J. A. Peters, Z. Liu, M. Sebastian, J. Im, T. C. Chasapis, A. C. Wibowo, D. Y. Chung, A. J. Freeman, B. W. Wessels and M. G. Kanatzidis, *Cryst. Growth Des.*, 2013, **13**, 2722.
19 H. S. Jung and N. G. Park, *Small*, 2015, **11**, 10.
20 S. D. Stranks, G. E. Eperon, G. Grancini, C. Menelaou, M. J. Alcocer, T. Leijtens, L. M. Herz, A. Petrozza and H. J. Snaith, *Science*, 2013, **342**, 341.
21 G. Xing, N. Mathews, S. Sun, S. S. Lim, Y. M. Lam, M. Gratzel, S. Mhaisalkar and T. C. Sum, *Science*, 2013, **342**, 344.

